

Wavelength Agile, Integrated Optical Transmitters for Analog Applications

L.A. Johansson, Chin-Hui Chen, Y.A. Akulova*, G.A. Fish* and L.A. Coldren

Department of Electrical and Computer Engineering
University of California, Santa Barbara, CA 93106

Tel: (805) 893-4543, Fax: (805) 893-7500, email: leif@ece.ucsb.edu

*Agility Communications, Inc., 600 Pine Ave, Santa Barbara, CA 93117

ABSTRACT

A summary of current work involving the development of high performance, wavelength-tunable integrated optical transmitters for analog applications is given. The performance of sampled-grating DBR lasers integrated with an SOA and an electroabsorption or Mach-Zehnder modulator is evaluated in terms of E/O conversion efficiency, noise performance and dynamic range. Optimization options to maximize either gain, noise figure or spurious-free dynamic range in analog link applications are discussed. It is shown how the combination of chip-scale integration and the use of bulk waveguide Franz-Keldysh absorption allows coupling of a large optical power level into the electroabsorption modulator, and its effects on the modulation response and analog link performance. Link results on an integrated SGDBR-SOA-EAM device includes a sub-octave SFDR in the 125 to 127 dB/Hz^{4/5} range and a broadband SFDR of 103-107 dB/Hz^{2/3} limited by third order intermodulation products or 95-98 dB/Hz^{1/2}, limited by second order intermodulation products, over a 1528 to 1573 nm wavelength range.

I. INTRODUCTION

Analog optical links have found applications areas such as wireless over fiber or antenna remoting for radar applications. In both cases, the optical link provides a low loss, wide band with medium, transparent to modulation format. The antenna units can be simplified, while system complexity can be located at a centralized location. The merging of WDM and wireless over fiber technologies will further enhance system reconfigurability and capacity, particularly for wireless over fiber applications [1]. Signal routing will enable dynamic allocation of radio resources and increased overall system capacity.

In this work, we have investigated the performance of an integrated photonic transmitter module based on a monolithically integrated InP chip comprising of a sampled-grating distributed Bragg grating (SG-DBR) laser, a semiconductor optical amplifier (SOA), and an electroabsorption modulator (EAM) or a Mach-Zehnder modulator (MZM), for high-performance analog optical link application. The paper is structured as follows. In section II, a brief overview of the SG-DBR laser platform that these analog transmitters are based upon is presented. In section III, the performance of transmitter including an EAM is reviewed. The performance of transmitters including a MZM is summarized in section IV, and the summary, section V gives a brief comparison of the performance of the two types of transmitters.

II. SG-DBR LASER PLATFORM

The devices are based on widely tunable SG-DBR lasers. The SG-DBR laser includes gain and phase sections positioned between two "sampled grating" distributed reflectors, sampled at different periods such that only one of their multiple reflection peaks can coincide at a time [2]. An offset quantum-well structure provides a platform for integration of the laser with other active regions, such as detectors or semiconductor optical amplifiers (SOA), and passive regions, such as phase or amplitude modulators. Typical performance of an SG-DBR laser integrated to an SOA is more than 10mW output power, lower than 2 MHz linewidth, and more than 40 dB sidemode suppression ratio over more than 40 nm wavelength tuning range [3].

The relative intensity noise (RIN) is produced both in the SG-DBR laser structure and in the SOA section. Fig. 3 shows the measured RIN spectra for an SG-DBR laser integrated to an SOA, for different values of gain section bias. The SOA bias was fixed at 180mA. At 200mA, the peak RIN is lower than -153 dB/Hz. The detector shot noise contribution has been subtracted in these graphs. The noise contribution of the SOA noise is best observed at frequencies away from the laser RIN peak, particularly below a few GHz, where the overall noise is limited by the SOA spontaneous emission. This effect observed in Fig. 3 by the compression of RIN level around 2GHz for gain section bias higher than 100mA. RIN measurements on SG-DBR lasers, not including an integrated SOA confirms a laser RIN level lower than -160 dB/Hz at frequencies away from the RIN peak [4].

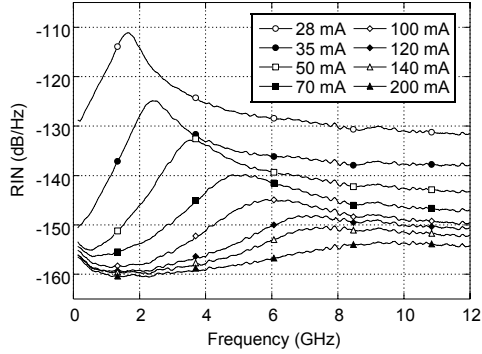


Fig. 1: Detected SG-DBR-SOA RIN spectra at 1552 nm for different values of gain section bias. SOA bias is fixed at 180 mA.

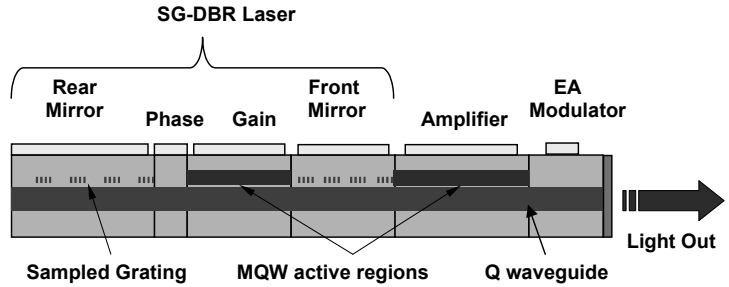


Fig 2. SG-DBR-SOA-EAM Device Schematic

III. EA TRANSMITTER

The integration of the laser and SOA active regions with the modulator section of the device has been accomplished by using an offset quantum-well structure [5]. In this integration technology the active region of the 250 μ m long modulator uses the same bulk quaternary waveguide as the tuning sections of the laser, show in Fig. 2. The Franz-Keldysh effect in the bulk waveguide material provides for larger spectral bandwidth as compared to the quantum-confined Stark effect. The composition of the bulk waveguide can be optimized to achieve high tuning efficiency for the laser and a target extinction ratio over the required wide spectral bandwidth for the modulator. The bulk design allows improved power handling of the device, avoiding carrier pileup problems or any degradation of the extinction. Further, integration eliminates the risk of input facet damage, shown to limit the available input optical power to waveguide p-i-n photodetectors to typically 200 mW. Here, the upper limit to coupled optical power is limited by Joule-heating of the device to 200mW I - V product, I being the EAM photocurrent. The efficient coupling between the source and the modulator/detector waveguide structure makes it convenient to study high optical power effects in the EAM device. The high operating waveguide power of the device is illustrated by Fig. 3, where the absorbed photocurrent, the EAM being biased for high extinction, is plotted against the output optical power, the EAM being biased for transmission. The photocurrent follows an almost perfectly linear relation to the waveguide optical power to photocurrents higher than 70 mA.

The variation in absorbed photocurrent with applied voltage can be modeled as an equivalent resistance [6]. The equivalent device conductance can be derived from reflection data obtained from a network analyzer and can be plotted as a function of fiber-coupled optical power, shown in Fig. 4. It is seen that the conductance varies linearly with the optical power and can be as high as 0.029 S, corresponding to only 34 Ω . The absorbed photocurrent affects the modulation response of the EAM. Normally, an optical modulator is assumed to have a high input impedance, therefore the RF to optical conversion efficiency is determined by the voltage slope efficiency and the parallel matching load, often 50 Ω , that is used for matching and providing a high bandwidth. In the presence of high optical waveguide power, the photocurrent will result in a compression of modulation sensitivity at lower frequencies, which in term will affect the bandwidth. Figure 5 shows the normalized modulation response at different transmitted optical power levels for an unterminated EAM. The 3-dB modulation bandwidth is shown to increase from 3.3GHz to closer to 8.0 GHz with optical power. Deriving the device conductance from the compression of the S21 measurements, there is good agreement compared to S11 data, also shown in Fig. 4.

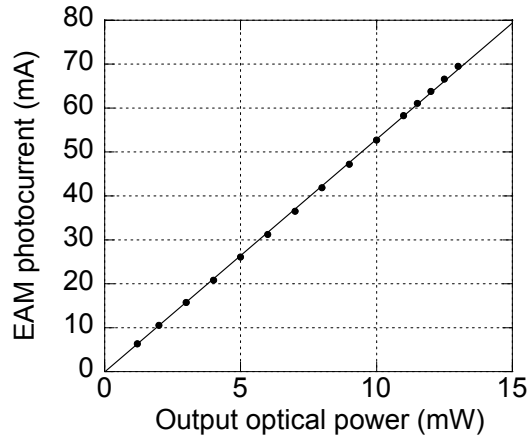


Fig. 3: DC photocurrent versus optical output power at 1558 nm. The EAM is biased at -2.8V for detection and unbiased for transmission.

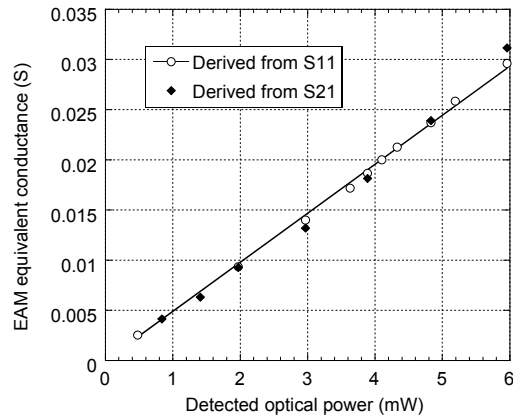


Fig. 4: Equivalent EAM conductance as a function of fiber-coupled transmitted optical power, derived from S-parameters, as a function of fiber-coupled transmitted power

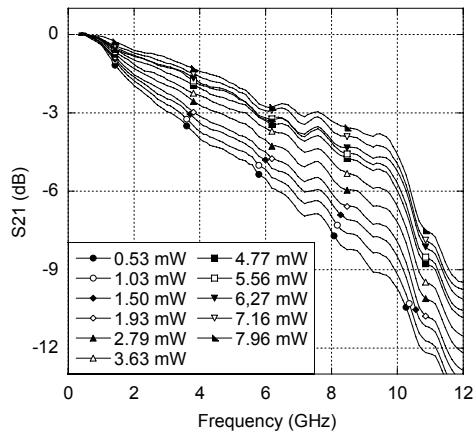


Fig. 5: Measured EAM modulation response for different levels of fiber-coupled transmitted optical power.

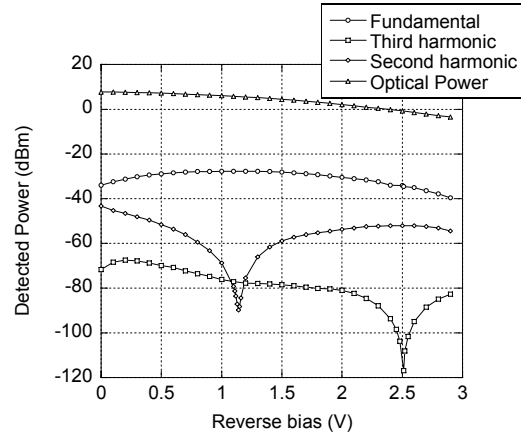


Fig. 6: Detected Optical power and RF power of fundamental and distortion products for 0 dBm modulation power.

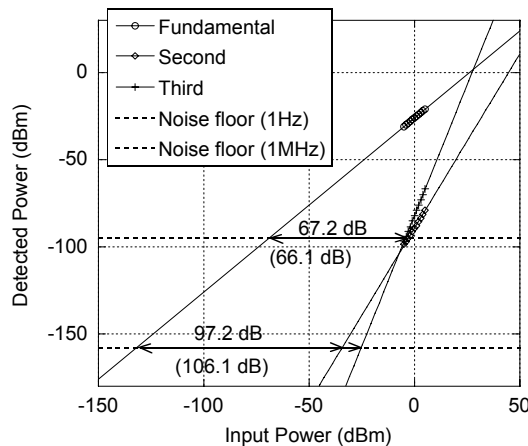


Fig. 7: Measured power of noise floor, fundamental, second and third order intermodulation products at 1552 nm, for -5 dBm to 5 dBm input RF power, 6.3mW optical power and -1.1V EAM bias. Broadband spurious-free dynamic range is also shown in 1Hz and 1MHz bandwidth.

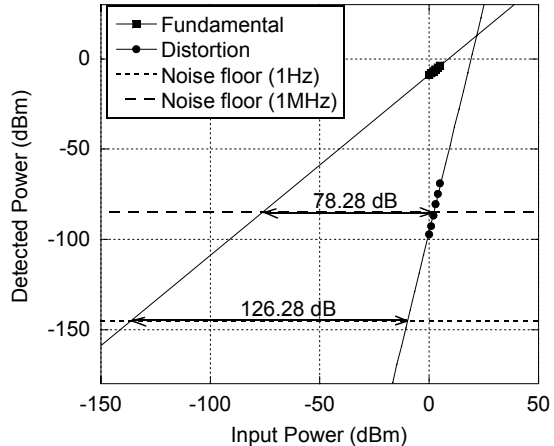


Fig. 8: Measured power of noise floor, fundamental and third order intermodulation products at 1552 nm, for 0 dBm to 5 dBm input RF power, 0.96mW optical power and -2.5V EAM bias. Sub-octave spurious-free dynamic range is also shown in 1Hz and 1MHz bandwidth.

The spurious-free dynamic range (SFDR) of the device is measured using two-tone modulation at 1 MHz offset of between -5 dBm to 8 dBm modulation power each. Fig. 6 shows the power of the fundamental, second and third harmonic intermodulation products as a function of EAM bias for 0 dBm modulation power of each carrier and at 0.5 GHz. Also shown in the plot is the optical output power, all for 100 mA bias current to gain and SOA sections at 1545 nm wavelength. Minimum second order distortion is observed at the bias point where the modulation efficiency is maximum, -1.1 V at 1545 nm. Minimum third order distortion appears at -2.5 V EAM bias voltage.

Figure 7 and 8 shows the broadband and sub-octave spurious-free dynamic range, both for 1Hz and 1MHz noise bandwidth. The broadband SFDR is taken at 1552 nm, 180mA bias current to gain section and SOA and at the bias point of minimum second order distortion. The noise level is -157 dBm/Hz, limited by shot noise and laser RIN. The SFDR limited by second order distortion is 97.19 dB in 1 Hz bandwidth and the SFDR limited by third order distortion is 106.09 dB in 1 Hz bandwidth, corresponding to 66.09 dB in 1 MHz bandwidth. Fig. 9 shows the broadband SFDR over the tuning range of the laser. The SFDR remains within a 103-107 dB/Hz^{2/3} range limited by third order intermodulation products, dominant for noise bandwidths above 1MHz, or 95-98 dB/Hz^{1/2} range limited by second order intermodulation products. The sub-octave SFDR is taken at 1552 nm, 180mA bias current to gain section, 120 mA SOA bias and at the bias point of minimum third order distortion. The noise floor is mainly limited by shot noise. The SFDR is 126.28 dB in 1 Hz bandwidth and remains within a 125-127 dB/Hz^{4/5} range, all limited by fifth order intermodulation products over the tuning range of the laser, Fig. 9.

The power of the distortion products relative to the fundamental and optimum EAM bias point for minimum distortion do not change significantly for modulation frequencies within the bandwidth of the modulator, up to 10 GHz for a 50Ω terminated device. This is shown in Fig. 10 where the measured SFDR is plotted as a function of modulation frequency over a range of 0.5 GHz to 10 GHz, both for 1 MHz noise bandwidth and normalized to 1 Hz. A 120μm long device was here used to provide sufficient bandwidth. Also shown in the figure is the combined effect of RIN and shot noise of the laser. It is seen that the frequency-dependent variation of the measured SFDR can be explained down to less than 2 dB margin by the RIN level, indicating relatively frequency independent linearity behavior of the EAM.

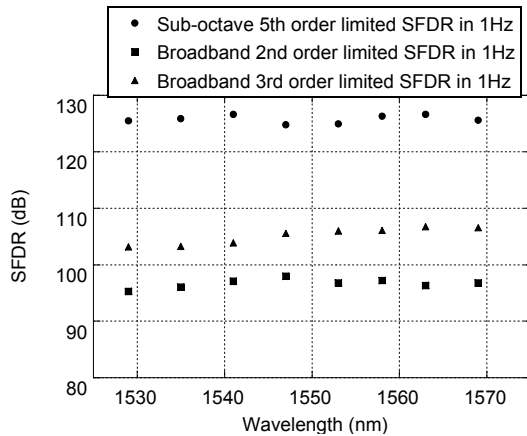


Fig. 9: Measured sub-octave and broadband spurious-free dynamic range, left scale, normalized to 1 Hz bandwidth for different wavelengths. Sub-octave SFDR limited by fifth order intermodulation products and broadband SFDR limited by second and third order intermodulation products.

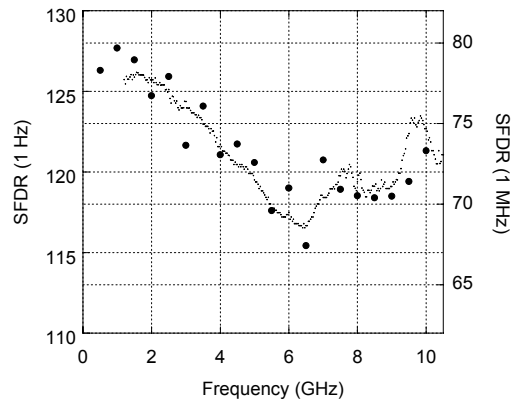


Fig. 10: Measured EAM SFDR versus modulation frequency for 1 MHz bandwidth and normalized to 1 Hz at 1554 nm. Also shown is relative effect on SFDR from the RIN level of the source.

Figure 11 shows the link gain and noise figure at 1 GHz as a function of EAM bias voltage at 1552 nm for 180 mA gain section bias and 180 mA SOA bias. The EAM was not terminated, while a 50Ω back-terminated 0.8A/W Discovery photodetector was used. The link gain peaks at -20.7dB between -1.4V and -1.5V EAM bias voltage. The gain can be somewhat improved by removing the back-termination of the detector, improving the gain by 6 dB gain, or using a high impedance receiver circuit. Reducing the transmitter fiber coupling loss will improve the gain further. However, ultimately to achieve optical link gain, the limitations imposed by the EAM photocurrent need to be addressed. With the assumption that a 50Ω signal source is used to modulate the EAM, increasing the waveguide optical power will only

allow an increase in link gain of 4.6 dB, limited by the available modulation current from the source, that can only change the waveguide optical power as much as corresponds to the absorbed photocurrent.

The link noise figure reaches its lowest level at a voltage different from where the link gain peaks. The reason for this is found in the RIN limited noise characteristic of the link. While the decreasing average output optical power at lower EAM bias will not change the level of the noise floor relative to optical power, the relative slope sensitivity will increase and so will then the modulated signal level, normalized by average transmitted power. There exists an optimum EAM bias for minimum noise figure where the improvements in relative slope sensitivity and the onset of shot noise limited noise performance balances out, here -2.4V resulting in 32.1dB NF. This phenomenon has been referred to as ‘low biasing’ the external modulator and has been observed using well-balanced Mach-Zehnder modulators [7]. In order to improve the noise figure of the optical link, a preamplifier should be used to overcome the link loss. Figure 12 shows the link noise figure and SFDR as a function of the amount of gain provided by the preamplification. As the gain is increased, the overall link noise figure is approaching that of the preamplifier, 2.4 dB . However, the use of preamplification will degrade the link SFDR because of the added distortion and noise of the amplifier. The added distortion is apparent at lower values of gain, where the noise floor is mainly dominated by laser and shot noise. A fifth order slope, such that was obtained in Fig. 8, is no longer found because of the added distortion of the amplifier, even though the output third order intercept point (OIP3) of the amplifier exceeded $+40\text{ dBm}$. As the gain of the preamplifier is increased, the noise floor is increasing in relative terms as it is getting limited by the amplifier noise, and the SFDR is degraded correspondingly.

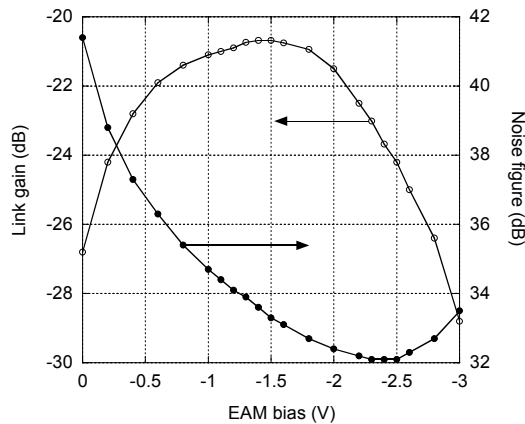


Fig. 11: Link gain and noise figure as a function of EAM bias voltage at 1552 nm for 180 mA gain section bias and 180 mA SOA bias.

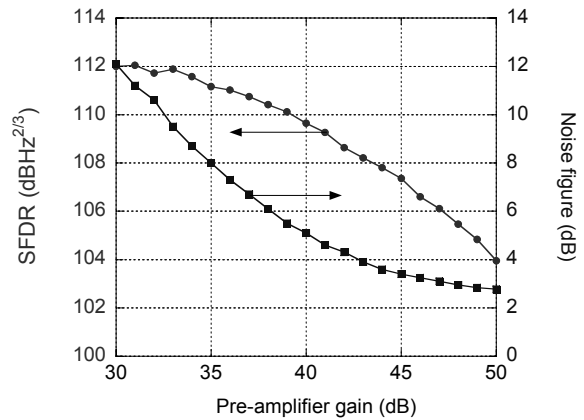


Fig. 12: SFDR and link noise figure for an pre-amplified electroabsorption-modulated optical link.

IV. MACH-ZEHNDER TRANSMITTER

The Mach-Zehnder modulator has a number of advantages compared to EA modulators. First of all, the RF link gain of a EA modulated optical link becomes limited by the absorbed photocurrent. MZ modulators do not have this limitation, being based on interferometric modulation. Second, by choosing inverting, non-inverting or a combined push-pull modulation, the modulator chirp can be controlled from positive to negative values. In terms of linearity, Mach Zehnder modulators have one disadvantage. With its sinusoidal response, the third order inflection points appear at the same bias point as zero slope sensitivity, limiting the available sub-octave SFDR.

Figure 13 shows a simple schematic of an SG-DBR laser integrated to an SOA and a Mach-Zehnder modulator. Since the MZ modulator is defined in the same material and with the same fabrication steps as the SG-DBR laser and SOA, the fabrication process is not much more complex than for the SG-DBR laser alone. The composition of the bulk waveguide can be optimized to achieve high tuning efficiency for the laser and a target V_p over the required wide spectral bandwidth for the modulator. The length of the electrodes of the Mach-Zehnder is in the $300\mu\text{m}$ to $700\mu\text{m}$ range.

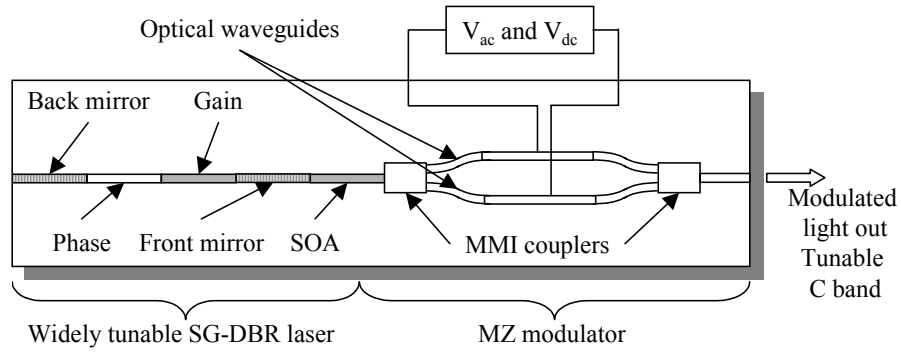


Fig. 13: Schematic overview of integrated SGDBR-SOA-MZM device.

Figure 14 shows a typical set of extinction curves for different values of phase difference between the arms of the Mach-Zehnder. In order to achieve high extinction, both the phase and the amplitude of the field passing through the arms of the Mach-Zehnder need to be matched. When both arms are biased around 0V, good extinction is achieved by design. When the phase offset is tuned to a different value, the available extinction ratio is obtained away from 0V and is degraded. The reason is the onset of Franz-Keldysh absorption in the bulk material. This can be a problem for digital applications and is the reason that it has been designed for good extinction around 0V. For analog applications, the altered response of the Mach-Zehnder can be taken advantage of in order to enhance the SFDR of the modulator. This is illustrated in Fig. 15 for 300 μ m electrode length, where the detected power of fundamental, second and third order intermodulation products are plotted as a function of MZ bias. As expected, the points of minimum second order distortion coincides with the point of maximum slope efficiency. However, unlike the typical Mach-Zehnder modulator, the points of maximum second order distortion, and therefore minimum third order distortion, do not coincide with minimum power of the fundamental. Therefore, by tuning the MZ bias point for minimum third order distortion, there is only about 3.3 dB penalty in the RF power of the fundamental, and optimized linearity for sub-octave applications is obtained. At this bias point, the sub-octave SFDR is 107.5 dB/Hz^{2/3}, limited by third order intermodulation products as shown in Fig. 16. The broadband SFDR is obtained by choosing the bias point where second order distortion has a minimum and is 92.8 dB/Hz^{2/3}, when limited by second order distortion or 103.6 dB/Hz^{2/3}, when limited by third order distortion products, as show in Fig. 17. In both cases, the noise floor was limited mainly by shot noise. It is worth noting that even though the fiber coupled output power of the MZ-devices, a peak 2mW, was much smaller than for the EA-devices, a peak 10mW, the broadband SFDR was comparable for both devices. MZ-devices with similar output power as the EA-devices should deliver improved broadband SFDR.

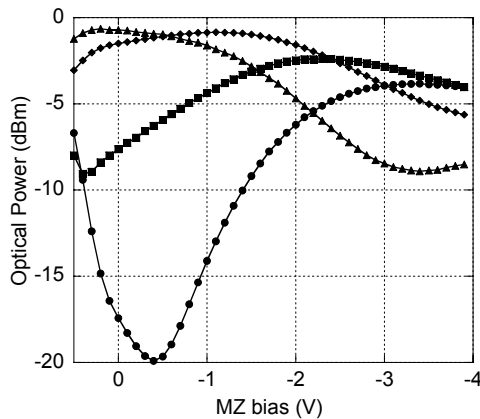


Fig. 14: Typical extinction curves for various differential MZ phase settings.

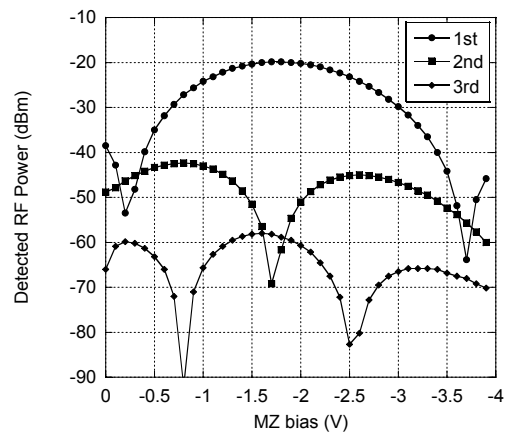


Fig. 15: Detected RF power of fundamental and intermodulation products for 0 dBm modulation power.

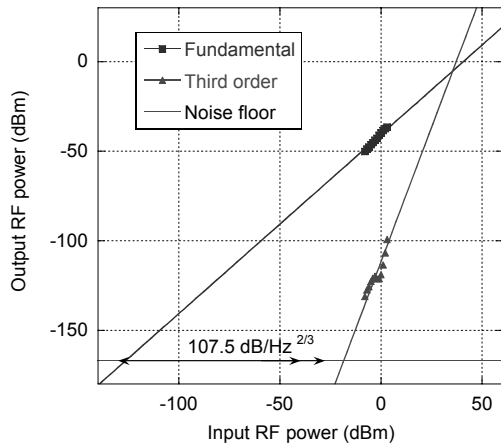


Fig. 16: Measured power of noise floor, fundamental and third order intermodulation products at 1547 nm.

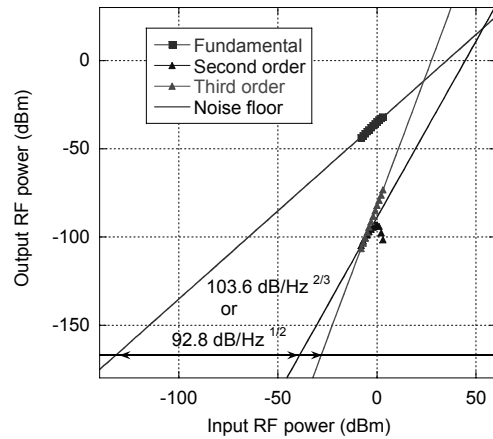


Fig. 17: Measured power of noise floor, fundamental, second and third order intermodulation products at 1547 nm.

A 700 μm electrode MZ-device was used for a link experiment, measuring link gain and noise figure. The longer electrode length was chosen to improve gain and noise figure in the absence of any preamplification. The link gain peaks at slightly above -30 dB, with an attributed noise figure of just below 35 dB. Again, despite that the peak output power is about five times lower for the MZ-devices than for the EA-devices, the link noise figure is comparable, mainly as a result of the steeper slope sensitivity of the long electrode MZ. A second contributing reason is the fact that this is an interferometric modulator, not as severely affected by that the absorbed photocurrent that had such a drastic impact on the response of the EA-devices. In fact, plotting the link gain on a linear scale as a function of received optical power, an almost perfect square relationship between link gain and power is obtained, indicating no compression of the modulator response with optical power. This relationship may be extrapolated at higher output power, such that a MZ-device with 10mW peak output power would have superior link performance of the corresponding EA-device.

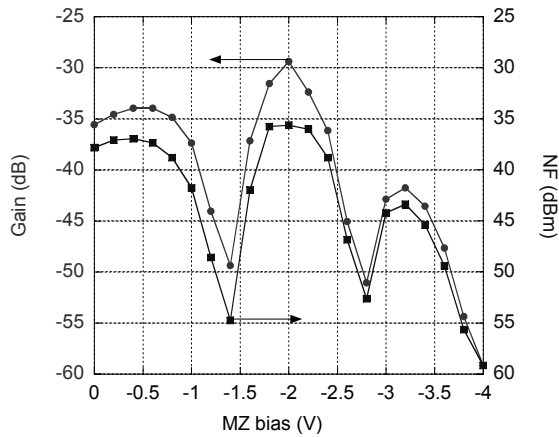


Fig. 18: MZ-modulated link gain and noise figure as a function of electrode bias point.

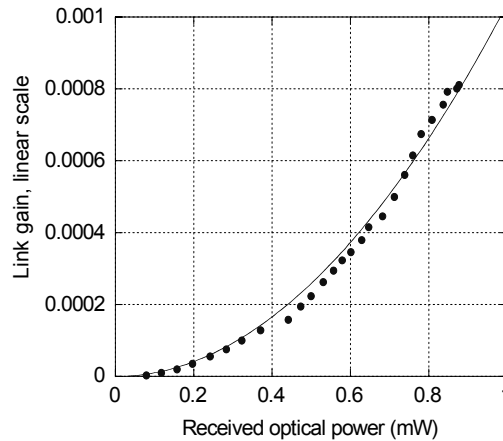


Fig. 19: MZ-modulated optical link gain as a function of received optical power.

V. SUMMARY

In this paper, SG-DBR laser based devices integrated to an SOA and either an electroabsorption modulator or a Mach-Zehnder modulator have been investigated for application as an analog transmitter. The performance has been evaluated in terms of spurious-free dynamic range, conversion efficiency and link noise figure. Using the EA device, a sub-octave SFDR of 126.3 dB/Hz^{4/5} and a broadband SFDR of 106.1 dB/Hz^{2/3} limited by third order intermodulation products or 97.2 dB/Hz^{1/2}, limited by second order intermodulation products is measured. A link gain up to -20.7 dB and noise figure up to 32.1 dB is also measured. It is also shown that the response of the EA-modulator is limited by the absorbed photocurrent. For the MZ-device, the broadband SFDR was slightly worse, 107.5 dB/Hz^{2/3}, mainly determined by the relatively lower output power of the MZ-device and the third order power dependence of the distortion. The broadband SFDR was comparable to the EA-modulator at 103.6 dB/Hz^{2/3} limited by third order intermodulation products or 92.8 dB/Hz^{1/2}, limited by second order intermodulation products. A link gain of -30 dB and noise figure of 35 dB is measured. These numbers would greatly benefit from higher output power as the MZ-modulator is not limited by photocurrent effects.

ACKNOWLEDGEMENTS

This work was in part funded by DARPA/MTO under the RFLICS program and in part under the CS-WDM program.

REFERENCES

1. C. Lim, A. Nirmalathas, M. Attygalle, D. Novak, R. Waterhouse, "The merging of a WDM fiber-radio backbone with a 25 GHz WDM ring network," *2003 IEEE MTT-S Microwave Symposium Digest*, vol.1, pp. 273 -276, June 8-1,3 2003.
2. V. Jayaraman, Z.-M. Chuang, L. A. Coldren, "Theory, Design, and Performance of Extended Tuning Range Semiconductor Laser with Sampled Grating", *IEEE J. of Quantum Electron.*, **29**, pp. 1824 -1834, 1993.
3. Y. A. Akulova, G. A. Fish, P. C. Koh, C. Schow, P. Kozodoy, A. Dahl, S. Nakagawa, M. Larson, M. Mack, T. Strand, C. Coldren, E. Hegblom, S. Penniman, T. Wipiejewski, and L. A. Coldren, "Widely-Tunable Electroabsorption-Modulated Sampled Grating DBR Laser Transmitter", *IEEE Journal on Selected Topics in Quantum Electronics*, **8**, pp. 1349-1357, 2002.
4. Hanxing Shi, D. Cohen, J. Barton, M. Majewski, L.A. Coldren, M.C. Larson and G.A. Fish, "Relative intensity noise measurements of a widely tunable sampled-grating DBR laser," *IEEE Photon. Technol. Lett.*, **14**, pp. 759-761, Jun 2002.
5. B. Mason, G. A. Fish, S. P DenBaars, and L. A. Coldren, "Widely tunable Sampled Grating DBR Laser with Integrated Electroabsorption Modulator", *IEEE Photon. Technol. Lett.*, **11**, pp. 638-640, 1999.
6. G.L. Li, P.K.L. Yu, W.S.C. Chang, K.K. Loi, C.K. Sun and S.A. Pappert, "Concise RF equivalent circuit model for electroabsorption modulators," *Electron. Lett.* **36**, pp. 818-820, 2000.
7. M. Farwell, W. Chang, and D. Huber, "Increased linear dynamic range by low biasing the Mach-Zehnder modulator," *IEEE Photon. Technol.Lett.*, **5** , pp. 779-782, Jul. 1993.